J|A|C|S
ARTICLES
Published on Web 07/03/2002

# Catalytic Role of Metal Ion in the Selection of Competing Reaction Paths: A First Principles Molecular Dynamics Study of the Enzymatic Reaction in Ribozyme

Mauro Boero,*[,†,‡] Kiyoyuki Terakura,[‡,§] and Masaru Tateno[‡]

*Contribution from the Angstrom Technology Partnership, Joint Research Center for Atom Technology, 1-1-1 Higashi, Tsukuba, Ibaraki 305-0046, Japan, National Institute of Advanced Industrial Science and Technology, Joint Research Center for Atom Technology, 1-1-1 Higashi, Tsukuba, Ibaraki 305-8562, Japan, and Research Institute for Computational Sciences, National Institute of Advanced Industrial Science and Technology, 1-1-1 Umezono, Tsukuba, Ibaraki 305-8568, Japan*

Received December 21, 2001

***Abstract:*** By using finite temperature first principles molecular dynamics, the mechanism of the enzymatic reaction of ribozyme was investigated for both the anionic and the radical charge states of the modeled RNA fragment. In the case of the anionic system, a pseudorotation and the subsequent 3′ → 2′ migration occur in a vacuum, rather than the self-cleavage of the phosphodiester. On the other hand, when either a divalent metal ion ($Mg^{2+}$) catalyst or the continuous hydrogen bond network of the solvent is present, the reaction path of the anionic species changes dramatically, going toward the transesterification channel. In a radical system, the transesterification can occur without a metal catalyst, as a consequence of the displacement of a *hole* (empty electronic state) along the reaction path. Thus, the present analysis suggests that a metal ion might be essential not only in lowering the activation barrier but also in selecting the reaction path among those corresponding to possible different charge states of the intermediate structure in vivo. Furthermore, simulation of the anionic species in solution shows that, in the absence of a metal catalyst, water molecules cooperate with the proton transfer via a proton wire mechanism and the hydrogen bond network plays a crucial role in preventing pseudorotations. On the other hand, when a metal cation is present in the vicinity of the site where the nucleophilic attack occurs, the hydrogen bond network is interrupted and detachment of the proton, enhanced by the catalyst, does not give rise to any proton-transfer process.

## Introduction

Since catalytic RNA molecules (ribozymes) were discovered about 20 years ago, they have gained enormous interest in molecular biology and medical science. The main reason is the fact that ribozymes can be engineered to cleave other target RNA molecules. Hence, they are very active agents able to inhibit gene expression and, for this reason, are very promising candidates in gene therapy of cancer.[1−6]

The fundamental chemical reaction operated by ribozymes is hydrolysis of the RNA phosphodiester, resulting in the cleavage of RNA at a particular target site (transesterification). The main steps of the transesterification, according to the most accredited reaction pathway, are summarized in the lower part of Scheme 1 from (1) to (3). However, changes in the environment, such as the pH of the solution, may favor other competing reaction channels. More specifically, in acidic conditions, the 3′ → 2′ phosphodiester migration reaction[7] is known to occur via a pseudorotation Ψ[8] that brings the system from the intermediate configuration 2 in Scheme 1 to a new orientation as in (4) (refer to the literature [1,9−13] for further details).

* To whom correspondence should be addressed. E-mail: mauro.boero@aist.go.jp.
† Angstrom Technology Partnership, Joint Research Center for Atom Technology.
‡ National Institute of Advanced Industrial Science and Technology.
§ National Institute of Advanced Industrial Science and Technology, Joint Research Center for Atom Technology.

(1) (a) Zhou, D.; Taira, K. *Chem. Rev.* **1998**, *98*, 991. (b) Takagi, Y.; Warashina, M.; Stec, W. J.; Yoshinari, K.; Taira, K. *Nucleic Acids Res.* **2001**, *29*, 1815. (c) Yoshinari, K.; Taira, K. *Nucleic Acids Res.* **2000**, *28*, 1730.
(2) Perreault, D. M.; Anslyn, E. V. *Angew. Chem., Int. Ed. Engl.* **1997**, *36*, 433 and references therein.
(3) (a) Buzayan, J. M.; Gerlach, W. L.; Bruening, G. *Nature* **1986**, *323*, 349. (b) Prody, G. A.; Bakos, J. T.; Buzayan, J. M.; Schneider, I. R.; Bruening, G. *Science* **1986**, *231*, 1577. (c) Hutchins, C. J.; Rathjen, P. D.; Forster, A. C.; Symons, R. H. *Nucleic Acids Res.* **1986**, *14*, 3627. (d) Hermann, T.; Auffinger, P.; Westhof, E. *Eur. Biophys. J.* **1998**, *27*, 153.
(4) (a) Joyce, G. F. *Science* **2000**, *289*, 401. (b) Schlutes, E. A.; Bartel, D. P. *Science* **2000**, *289*, 448.
(5) (a) Santoro, S. W.; Joyce, G. F. *Proc. Natl. Acad. Sci. U.S.A.* **1997**, *94*, 4262. (b) Steitz, T. A.; Steitz, J. A. *Proc. Natl. Acad. Sci. U.S.A.* **1993**, *90*, 6498. (c) Zhang, B.; Cech, T. R. *Chem. Biol.* **1998**, *5*, 539. (d) Bramlage, B.; Luzi, E.; Eckstein, F. *Trends Biotechnol.* **1998**, *16*, 434.
(6) Kuwabara, T.; Warashima, M.; Taira, K. *Trends Biotechnol.* **2000**, *18*, 462.
(7) We adopt the standard notation in which atoms are numbered from 1 to 5 on the ribose ring starting from the base, here replaced by a H atom.
(8) (a) Westheimer, F. H. *Acc. Chem. Res.* **1968**, *1*, 70. (b) Cramer, C. J. *J. Am. Chem. Soc.* **1990**, *112*, 7965. (c) Cramer, C. J.; Gustafson, S. M. *J. Am. Chem. Soc.* **1993**, 115, 9315. (d) Cramer, C. J.; Gustafson, S. M. *J. Am. Chem. Soc.* **1994**, *116*, 723. (e) Taira, K. *Prog. Synth. Oligonucleotides* **1995**, *II*, 1323 (in Japanese).

*Scheme 1*

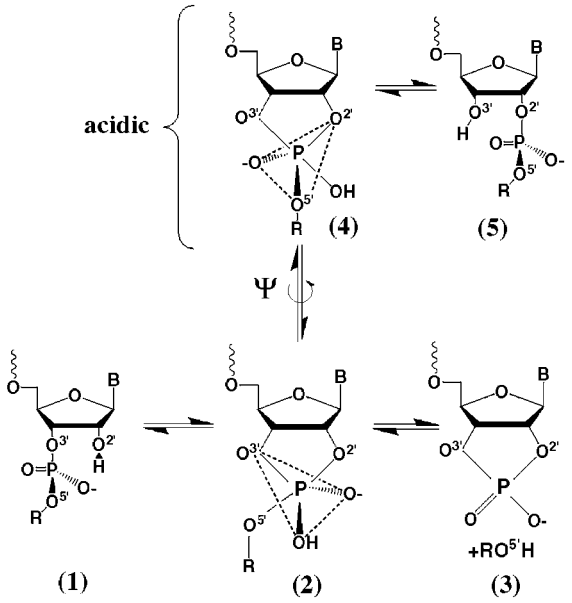


Despite extensive efforts, the intimate details of the reaction mechanism governing the transesterification still represent a challenge. To date, they have been deduced on the basis of assumptions and static quantum calculations on very simplified models and all the reported quantum calculations did not include electron correlation beyond a posteriori semiempirical energy corrections.[10−12] Furthermore, the presence of the ribose ring, the finite temperature dynamical effects, and the influence of the solvent in which the actual reaction occurs were never considered.

Recent progress in computer facilities and software algorithms make it only now possible to study in great detail rather complicated chemical reactions.[14] This opens new possibilities in elucidating the basic aspects of the reaction and, in a longer term perspective, in predicting reaction rates and in addressing improvements in the molecular engineering phase.

In the present work, we investigate via first principles molecular dynamics the effects of the charge state of the phosphate in the reaction process, the role of a divalent metal ion in enhancing the transesterification process, and the crucial features due to the inclusion of the solvent. Furthermore, we work out the related activation barriers in an attempt to address the problem of the formation of a transition state or an intermediate metastable structure, which represents a still unresolved issue. The basic chemistry of the phosphate as provided by the calculations *in a vacuum* represents a clear picture of the fundamental reaction mechanism.[10−12] On the other hand, the inclusion of the solvent reveals that the anionic species, known to be the dominating species in physiological environments,[1−2] benefits from the presence of a hydrogen bond network: H-bonds slow the pseudorotation observed in a vacuum, and a *proton wire* mechanism[15] responsible for the proton transfer in the nucleophilic attack phase in the absence of a divalent cation is evidenced for the first time, providing new insight in the transesterification mechanism of non-metalloenzymes. In contrast, when a $Mg^{2+}$ is present in the vicinity of the $O^{2'}$ site, the H-bond network is interrupted and the metal forms a solvation shell including $O^{2'}$ and four or five water molecules. As a consequence, no proton transfer occurs, in agreement with the experimental evidence.[16] These results underscore the reiterated arguments about the importance of water in simulating biological systems.[17]

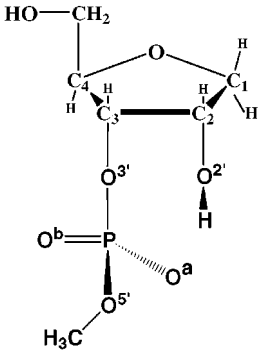


***Figure 1.*** RNA system, extracted from a regular RNA, used in the simulations. All atoms are labeled according to the standard notations. The atom labeled $O^a$ corresponds to $O^-$ in panel 1 of Scheme 1.

## Computational Method

We adopted a density functional theory (DFT) approach[18] with gradient corrections on exchange and correlation after Hamprecht, Cohen, Tozer, and Handy (HCTH)[19] which has been shown to perform as good as (and in some cases better than) the hybrid B3LYP functional.[20,21] We performed dynamical simulations within the Car−Parrinello[22,23] (CP) scheme. We used a system consisting of a single RNA ribose unit as shown in Figure 1, amounting to 26 atoms, in a cubic supercell of side $L = 14.817$ Å with periodic boundary conditions. Such a relatively large size ensures a good separation of the system from its periodically repeated images. Troullier−Martins[24] norm-conserving pseudopotentials were used to account for the valence−core interactions, and valence wave functions were expanded in plane waves with an energy cutoff of 70 Ry. In the case of the open-shell

(9) (a) Nissen, P.; Hansen, J.; Ban, N.; Moore, P. B.; Steitz, T. A. *Science* **2000**, *289*, 920. (b) Muth, G. W.; Ortoleva-Donnelly, L.; Strobel, S. A. *Science* **2000**, *289*, 947.
(10) Uchimaru, T.; Tanabe, K.; Nishikawa, S.; Taira, K. *J. Am. Chem. Soc.* **1991**, *113*, 4351.
(11) (a) Dejaegere, A.; Lim, C.; Karplus, M. *J. Am. Chem. Soc.* **1991**, *113*, 4353. (b) Lim, C.; Karplus, M. *J. Am. Chem. Soc.* **1990**, *112*, 5872.
(12) (a) Storer, J. W.; Uchimaru, T.; Tanabe, K.; Uebayashi, M.; Nishikawa, S.; Taira, K. *J. Am. Chem. Soc.* **1991**, *113*, 5216. (b) Yliniemela, A.; Uchimaru, T.; Tanabe, K.; Taira, K. *J. Am. Chem. Soc.* **1993**, *115*, 3032. (c) Uchimaru, T.; Stec, W. J.; Tsuzuki, S.; Hirose, T.; Tanabe, K.; Taira, K. *Chem. Phys. Lett.* **1996**, *63*, 691.
(13) Roussev, C. D.; Ivanova, G. D.; Bratovanova, E. K.; Vassilev, N. G.; Petkov, D. D. *J. Am. Chem. Soc.* **1999**, *121*, 11267.
(14) (a) Hutter, J.; Carloni, P.; Parrinello, M. *J. Am. Chem. Soc.* **1996**, *18*, 8710. (b) Alber, F.; Folkers, G.; Carloni, P. *J. Mol. Struct. (THEOCHEM)* **1999**, *489*, 237. (c) Carloni, P.; Sprik, M.; Andreoni, W. *J. Phys. Chem. B* **2000**, *104*, 823. (d) Boero, M.; Parrinello, M.; Terakura, K. *J. Am. Chem. Soc.* **1998**, *120*, 2746. (e) Boero, M.; Parrinello, M.; Hüffer, S.; Weiss, H. *J. Am. Chem. Soc.* **2000**, *122*, 501. (f) Alber, F.; Carloni, P. *Protein Sci.* **2000**, *9*, 2535.
(15) Pomès, R.; Roux, B. *J. Phys. Chem.* **1996**, *100*, 2519.
(16) Sawata, S.; Komiyama, M.; Taira, K. *J. Am. Chem. Soc.* **1995**, *117*, 2357.
(17) Gerstein, M.; Levitt, M. *Sci. Am.* **1998**, (Nov),100.
(18) Kohn, W.; Sham, L. J. *Phys. Rev.* **1965**, *140*, A1133.
(19) Hamprecht, F. A.; Cohen, A. J.; Tozer, D. J.; Handy, N. C. *J. Chem. Phys.* **1998**, *109*, 6264.
(20) (a) Boese, A. D.; Doltsinis, N. L.; Handy, N. C.; Sprik, M. *J. Chem. Phys.* **2000**, *112*, 1670. (b) Cohen, A. J.; Handy, N. C. *Chem. Phys. Lett.* **2000**, *316*, 160. (c) Ahlrichs, R.; Furche, F.; Grimme, S. *Chem. Phys. Lett.* **2000**, *325*, 317. (d) Raugei, S.; Klein, M. L. *J. Am. Chem. Soc.* **2001**, *123*, 9484.
(21) The fact that the HCTH functional includes the PW91 correlation (Perdew, J. P.; Wang, Y. *Phys. Rev. B* **1992**, *45*, 13244) represents an improvement in the description of dispersion terms (Tsuzuki, S.; Lüthi, H. P. *J. Chem. Phys.* **2001**, *114*, 3949), which are generally difficult to treat at any DFT level.
(22) Car, R.; Parrinello, M. *Phys. Rev. Lett.* **1985**, *55*, 2471.
(23) CPMD code by J. Hutter et al. at MPI für Festkörperforschung and IBM Zurich Research Laboratory, 1990−2000.
(24) Troullier, N.; Martins, J. L. *Phys. Rev. B* **1991**, *43*, 1993.

***Table 1.*** Main Phosphorus−Oxygen Distances for the Different Charge State[a]

| | anion | radical |
|---|---|---|
| spin state | singlet | doublet |
| P−O[a] | 1.492 | 1.515 |
| P−O[b] | 1.497 | 1.508 |
| P−O[3′] | 1.703 | 1.635 |
| P−O[5′] | 1.652 | 1.598 |

[a] The labeling of the oxygen atoms around P is the same adopted in Figure 1. Distances Are Expressed in angstroms.

calculations, local spin density approximation (LSDA) on exchange and correlation within the same HCTH framework was adopted.

The system in solution was simulated by first equilibrating an NVT ensemble of 72 water molecules at standard temperature (300 K) and density (1.0 g/cm$^3$) in a cubic supercell of side $L = 13.146$ Å with periodic boundary conditions. Then we cleaved a space to allocate the rybozyme model system forming an ensemble consisting of this same system plus 62 water molecules. The temperature was controlled via a Nosé−Hoover thermostat chain.[25] An integration step of 4 au (0.0967 fs) and a fictitious electron mass of 1200 au ensured good control of the conserved quantities.

The free energy profiles were calculated within the Blue Moon ensemble theory,[26] by using the distance between the phosphorus atom and the O$^{2'}$ oxygen as a reaction coordinate. Equilibration times of ∼2.0 ps for each sampled constraint ensured a meaningful statistics. Total and free energy estimations are affected by an average error bar of ∼2.0 kcal/mol, which is the typical accuracy allowed by present-day first principles approaches.

## Results and Discussion

We took the RNA structure as obtained from standard crystallographic data and constructed the system reported in Figure 1 by replacing the subsequent ribose unit with a methyl group (Me) and by substituting the base with a hydrogen atom. This system has locally all the properties of a single RNA unit and fully represents the active part of a typical ribozyme.[27] It may be stressed that the two oxygen atoms indicated as O$^a$ and O$^b$ in Figure 1 are geometrically and electronically equivalent in both the anion and the radical species. This is clearly shown by both the geometrical data of Table 1 and the spin density and electron localization function (ELF)[28] distribution (not shown).

The preequilibration phase of the system in a vacuum at 300 K (∼1.2 ps) led to the formation of an intramolecular hydrogen bond (IMHB) between the H atom of the O$^{2'}$H group and O$^a$. However, in solution, this does not hold as discussed later.

In the following paragraphs, we first investigate the reaction mechanism of the anionic RNA system in a vacuum, for which previous static calculations at the Hartree−Fock (HF) level on more simplified model systems are available for comparison.[8−10,29] Then we inspect the role of $Mg^{2+}$ in enhancing the reaction rate and in tuning the reaction channel.[30,31] Furthermore, we also analyze the reaction path of the radical species in an attempt to rationalize the effects of temperature and charge state on the phosphodiester site. In aqueous solution, it is experimentally known[1,2] that the dominant catalytic species is an anion. However, it has been argued that a sufficiently hydrated pentacoordinated P may exist in any charge state.[12(a,b)]

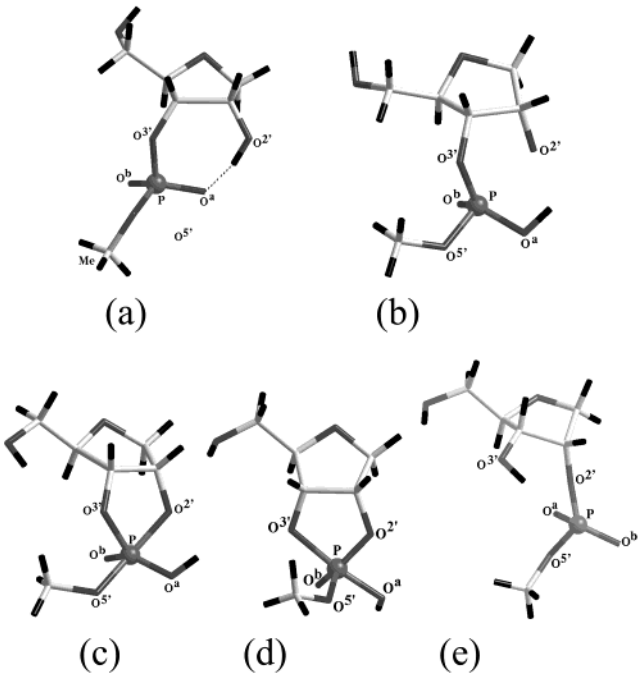


***Figure 2.*** Snapshots of the main phases of the 3′ → 2′ phosphodiester migration: (a) the initial system, (b) the system after the O$^{2'}$ → O$^a$ proton transfer, (c) the TBP formed close to the transition state, (d) the transition state in which a pseudorotation occurred, and (e) the final product. The color code for the sticks is black for H, light gray for C, and dark gray for O. P is evidenced by a ball for sake of clarity.

Moreover, it is also interesting per se to look at different charge states and to analyze their consequences in the reaction mechanism, since this has both structural and electronic implications.

**1. The Anionic System.** We sampled the reaction path that leads to the formation of the trigonal bipyramidal phosphorane (TBP)[1,13] structure 2 in Scheme 1 by using the distance $\xi = |P-O^{2'}|$ as a reaction coordinate. In the anionic species, the number of occupied $\alpha$ spin states is equal to the number of occupied $\beta$ states; thus, the system is in a singlet state.

By looking at the reaction path, a first feature that can be noticed is the proton transfer[32] from O$^{2'}$ (Figure 2a) to one of the two *dangling* O bound to P (O$^a$ in the present case) occurring when the P−O$^{2'}$ shrinks to 2.30 Å. The proton of the O$^{2'}$H group jumps on O$^a$ and forms a stable O−H bond (Figure 2b).[2,31] A TBP is then formed at $\xi = 1.80$ Å (Figure 2c), and no IMHB between this H and O$^{2'}$ is kept. This TBP structure undergoes a spontaneous pseudorotation as in Scheme 1 as soon as the transition state (TS) is reached. The atoms O$^{2'}$ and O$^{5'}$ are initially in apical positions and O$^{3'}$, O$^a$, and O$^b$ occupy the equatorial vertexes of the TBP. However, as long as the dynamics proceeds, O$^{5'}$ moves out of the axial position and a

(25) (a) Nosé, S. *Mol. Phys.* **1984**, *52*, 255. (b) Nosé, S. *J. Chem. Phys.* **1984**, *81*, 511. (c) Hoover, W. G. *Phys. Rev. B* **1985**, *31*, 1695.
(26) Sprik, M.; Ciccotti, G. *J. Chem. Phys.* **1998**, *109*, 7737 and refernces therein.
(27) (a) Pley, H. W.; Flaherty, K. M.; McKay, D. B. *Nature* **1994**, *372*, 68. (b) Burke, J. M. *Nat. Struct. Biol.* **2001**, *8*, 382.
(28) (a) Becke, A. D.; Edgecombe, K. E. *J. Chem. Phys.* **1990**, *92*, 5397. (b) Chesnut, D, B.; Savin, A. *J. Am. Chem. Soc.* **1999**, *121*, 2335.
(29) Lim, C.; Tole, P. *J. Am. Chem. Soc.* **1992**, *114*, 7245.
(30) (a) Dahm, S. C.; Derrick, W. B.; Uhlenbeck, O. C. *Biochemistry* **1993**, *32*, 13040. (b) Pyle, A. M. *Science* **1993**, *261*, 709. (c) Scott, W. G.; Murray, J. B.; Arnold, J. R. P.; Stoddard, B. L.; Klug, A. *Science* **1996**, *274*, 2065. (d) Zhou, D. M.; Taira, K. *Proc. Natl. Acad. Sci. U.S.A.* **1997**, *94*, 14343. (e) Kuimelis, R. G.; McLaughlin, L. W. *Chem. Rev.* **1998**, *98*, 1027. (f) Torres, R. A.; Bruice, T. C. *J. Am. Chem. Soc.* **2000**, *122*, 781.
(31) Taira, K. Private communication.
(32) (a) Kuusela, S.; Lönnberg, H. *Curr. Top. Solution Chem.* **1997**, *2*, 29. (b) Oivanen, M.; Kuusela, S.; Lönnberg, H. *Chem. Rev.* **1998**, *98*, 961. (c) Mavri, J.; Berendsen, J. C. *J. Phys. Chem.* **1995**, *99*, 12711.

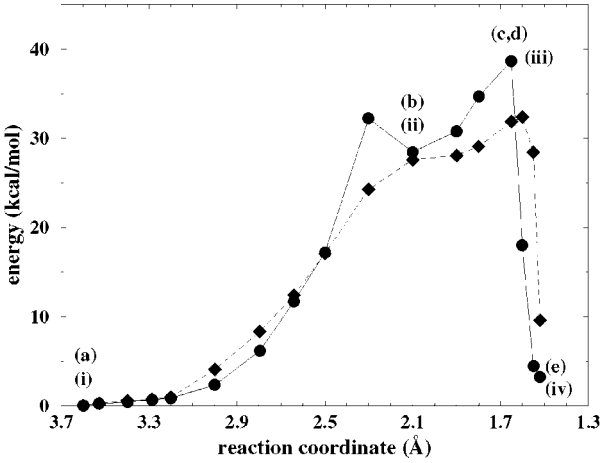


***Figure 3.*** Free (diamonds) and total (circles) energy profiles as a function of the reaction coordinate for the anionic system. The labels from (a) to (e) indicate the geometries reported in the snapshots of Figure 2, while labels from (i) to (v) refer to the electronic structure represented in Figure 4 (see text for details).

new arrangement presenting $O^{3'}$ and $O^{a}$ (on average) in apical positions with $O^{2'}$, $O^{b}$, and $O^{5'}$ on the equatorial plane is formed (Figure 2d).

In these conditions, the system is in the TS identified by the maximum at $\xi = 1.64$ Å in the free and total energy profiles (Figure 3). Hence, the two bonds P−$O^{3'}$ and P−$O^{a}$ start competing until P−$O^{3'}$ eventually breaks. Dynamical rearrangements of the phosphodiester, transferred from $O^{3'}$ to $O^{2'}$, and the simultaneous rotation of $O^{a}$, $O^{b}$, and $O^{5'}$ around the P−$O^{2'}$ axis bring the H close to the now unsaturated $O^{3'}$. Thus, $O^{3'}$ takes the proton as in Figure 2e and the phosphodiester migration process is completed. This final proton transfer occurs spontaneously at the end of the process (point e, iv in Figure 3) and is responsible for the lower value of the total energy curve with respect to the free energy profile. On the other hand, this proton transfer is not taken into account in our sampled reaction coordinate; hence, it does not contribute to the free energy.[33]

The computed activation energy for the 3′ → 2′ transfer process is $\Delta E = 38.7 \pm 2.2$ kcal/mol and $\Delta F = 32.4 \pm 2.2$ kcal/mol, significantly high, and the transesterification does not occur spontaneously.

To get a better insight into the occurrence of the pseudorotation, we monitored the Kohn−Sham (KS) occupied and unoccupied energy levels and the corresponding space evolution of the doubly occupied HOMO. The system remains in the closed-shell configuration along the whole reaction path. The KS energy gap is 3.81 eV at the beginning of the reaction ($\xi =$ 3.40 Å), and then it shrinks to 3.12 eV at the transition state point and eventually enlarges again to 3.74 eV at the end of the reaction, almost back to its original value. This is not surprising, being the product the symmetric image of the reactant.

More specifically, the HOMO charge sits equivalently on both $O^{a}$ and $O^{b}$ at the beginning of the process (Figure 4i). When the proton transfer occurs (Figure 4ii), part of the electronic charge is still located on $O^{b}$, but the main contribution has moved to $O^{2'}$, which is now carrying most of the negative charge. At the transition state of Figure 4iii ($\xi = |P-O^{2'}| =$ 1.65 Å, $|P-O^{3'}| = 1.69$ Å), the negative charge of the system is distributed again on $O^{b}$, but nonnegligible amplitudes are present on both $O^{2'}$ and $O^{5'}$. This is confirmed also by the atomic charges computed from the Mulliken population analysis (Table 2).

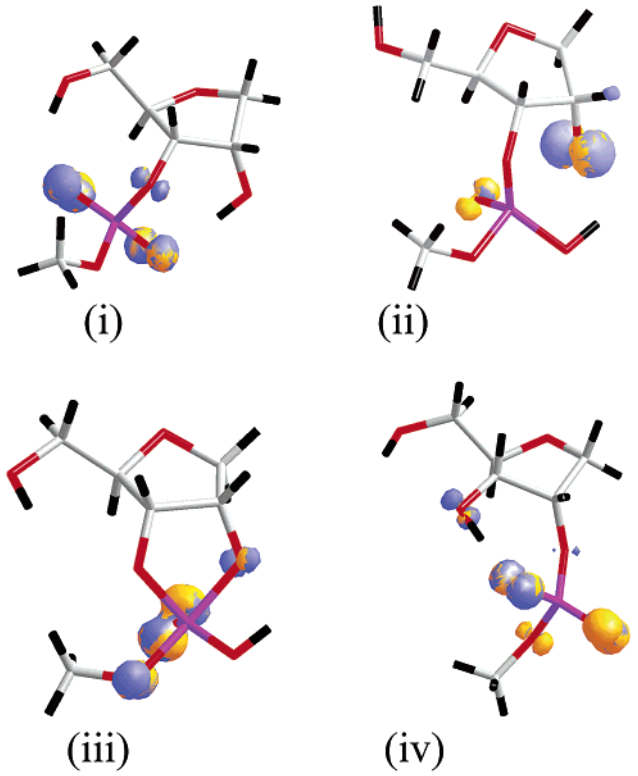


***Figure 4.*** Snapshots of the doubly occupied HOMO during the reaction. The initial state (i), the system after the proton transfer (ii), the transition state (iii), and the final product (iv). These same labels are reported along the energy profiles in Figure 3. The color code is black for H, red for O, gray for C, and purple for P. Squared modulus wave functions are shown as isosurfaces at $6 \times 10^{-4}$ e/Å$^3$. Yellow is used for the α spin component and blue for the $\beta$ spin component.

***Table 2.*** Mulliken Atomic Charges on P and O Atoms of the Pentacoordinated P at the Various Transition States[a]

| atom | anion | anion with $Mg^{2+}$ | radical |
|---|---|---|---|
| P | +2.38 | +1.86 | +2.12 |
| $O^{2'}$ | −0.73 | −0.36 | −0.55 |
| $O^{3'}$ | −0.39 | −0.44 | −0.59 |
| $O^{5'}$ | −0.76 | −0.51 | −0.62 |
| $O^{a}$ | −0.52 | −0.56 | −0.70 |
| $O^{b}$ | −1.16 | −0.54 | −0.89 |

[a] The atom labeling is the same as in Figure 1.

The pseudorotation, i.e., the conformational change from (c) to (d) in Figure 2, occurs after $\xi$ is reduced to a value corresponding to the transition state.

The above charge analysis can provide a hint about the trigger of the pseudorotation: if $O^{5'}$ rotates out of the plane containing $O^{2'}$, $O^{3'}$, and P, then $O^{5'}$ and $O^{2'}$ no longer occupy the axial positions of the TBP, but two of the equatorial vertexes (see Chart 1), minimizing the electrostatic repulsion. In the new arrangement, the former long P−$O^{2'}$, strongly ionic in the axial position, becomes slightly shorter than P−$O^{3'}$ as reported above. Thus, the character of the two bonds is exchanged: P−$O^{2'}$ shifts toward a more covalent character, while P−$O^{3'}$ becomes more ionic. This is suggested also by the Mulliken charge of those

(33) See, for example: Boero, M., Morikawa, Y.; Terakura, K.; Ozeki, M. *J. Chem. Phys.* **2000**, *112*, 9549.

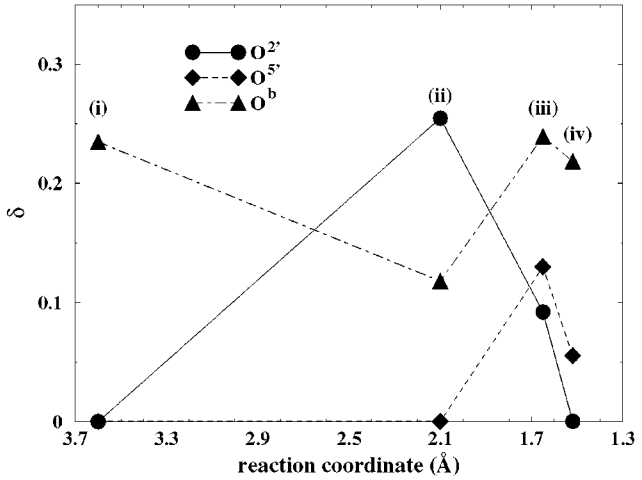


***Figure 5.*** Distribution of the HOMO partial charge $\delta$ on $O^{2'}$, $O^{5'}$, and $O^{b}$ along the reaction coordinate. Details and definition of $\delta$ are given in the text.

***Chart 1***

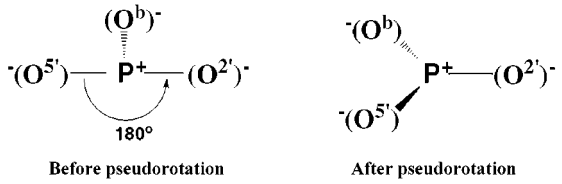


two atoms in Table 2. The final electronic structure (Figure 4iv), with $O^{a}$ and $O^{b}$ carrying the HOMO electron density, is the mirror image of the initial system, underscoring the fact that the simple transfer of the phosphodiester from $O^{3'}$ to $O^{2'}$ does not alter the chemistry around P. The HOMO charge evolution for the most relevant oxygen atoms is quantified and summarized in Figure 5, where the amount of HOMO wave function density

$$\delta = \int_{\Sigma} |\Psi_i(\vec{r})|^2 d^3r \qquad (1)$$

projected into a sphere $\Sigma$ is plotted against the reaction coordinate. The spheres $\Sigma$ are centered on each O atom bound to P and have as a radius half of the corresponding P−O bond.

**2. The Catalytic Role of $Mg^{2+}$.** It is experimentally well known that a large majority of ribozymes, such as hammerhead ribozymes, require divalent metal cations to be active.[5b,29] We therefore examined the catalytic role of a divalent metal ion by calculations on this same anionic system including a $Mg^{2+}$ cation in the vicinity (∼2.5−2.3 Å) of $O^{5'}$. The results of our simulations, discussed below, have shown that the transesterification occurs and that a pseudorotation is prevented whenever a metal cation is present.

In our system, the actual catalytic site turned out to be characterized by a $Mg^{2+}$−$O^{5'}$ distance of ∼2.0 Å, corresponding to a local minimum of the electrostatic potential. We performed constrained dynamics simulations by starting, either with the $Mg^{2+}$ on the $O^{5'}$−P−$O^{3'}$ plane, closer to $O^{3'}$ (Mg−$O^{3'}$ = 2.30 Å, Mg−$O^{5'}$ = 2.90 Å) or with the metal on the $O^{5'}$−P−$O^{2'}$ plane, closer to $O^{2'}$ (Mg−$O^{2'}$ = 2.30 Å, Mg−$O^{5'}$ = 3.2 Å). In both cases, the metal cation displaces close to $O^{5'}$ in such a way that $Mg^{2+}$−$O^{5'}$ becomes ∼2.0 Å. Once this situation is stabilized, the reaction path switched rapidly toward the *catalytic cleavage* of the P−$O^{5'}$ bond. The proton transfer from $O^{2'}$ to $O^{a}$ occurs in a way very similar to the reaction in a vacuum in the absence of the divalent metal ion.

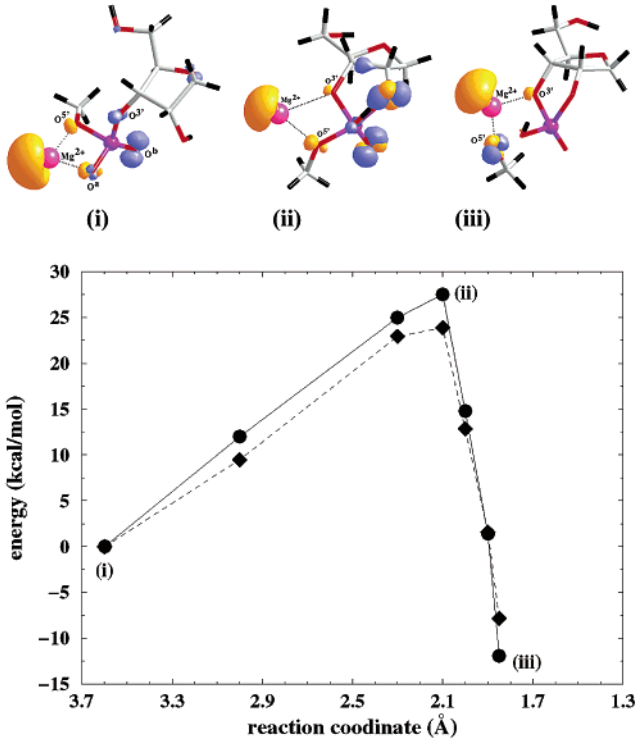


***Figure 6.*** Snapshots (upper panel) and total and free energy profiles (lower panel) of the cleavage reaction of the anionic species catalyzed by $Mg^{2+}$. The Mg atom is represented as a pink ball and labels i−iii indicate the corresponding points along the energy curves. The isosurfaces at $6 \times 10^{-4}$ e/Å$^3$ represent the LUMO (yellow) that becomes partially filled during the reaction and the HOMO (blue).

This conclusion about the catalytic role of the divalent metal ion was further supported by an *unconstrained* dynamics calculation in which the TS ($\xi_{TS}$ = 2.10 Å) of the anion was used as a starting structure. We released the P−$O^{5'}$ constraint and performed ∼1-ps dynamics starting with $Mg^{2+}$ closer (2.20 Å) to $O^{2'}$ than to $O^{5'}$ (3.10 Å). Again, the result was a displacement of the metal catalyst closer to $O^{5'}$ and the cleavage of the P−$O^{5'}$ bond, while P−$O^{2'}$ and P−$O^{3'}$ remain unaffected.

On the other hand, a similar calculation for a reaction coordinate value slightly before the TS value ($\xi$ = 2.20 Å) has shown that, after the release of the constraint, the phosphodiester breaks the P−$O^{2'}$ bond, not yet fully formed, and reverts rapidly (∼0.6 ps) to a structure similar to the reactant of Figure 2a.

The most remarkable differences with respect to the absence of the metal catalyst can be summarized as follows: (i) the activations barriers ($\Delta E$ = 27.6 ± 2.0 kcal/mol, $\Delta F$ = 23.9 ± 1.9 kcal/mol) lower dramatically, and (ii) the cleavage of the P−$O^{5'}$ bond takes place (see Figure 6). These results suggest that the catalytic role played by the divalent metal ion is the hindrance of pseudorotations of the TBP and the selection of the transesterification reaction path.

Although in solution a five-membered cyclic phosphate, like the one of Figure 6iii, is known to be unstable and to be hydrolyzed, in a vacuum the electrostatic gain due to the interaction of $Mg^{2+}$ and $CH_3O^-$ is responsible for the stabilization of the product. We remark that the presence of the solvent changes drastically the scenario depicted in a vacuum,[16] as discussed later. However, it does not alter either the basic feature of the

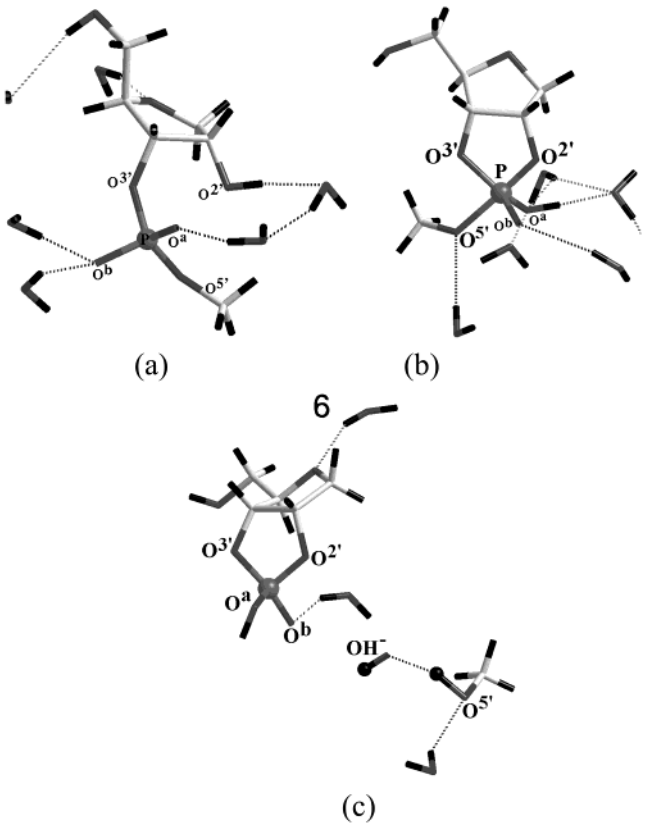


***Figure 7.*** Snapshots of the main phases of the reaction in solution: (a) the initial configuration, (b) the metastable intermediate, and (c) the final product with the leaving $O^{5'}$ group that has given rise to hydrolysis. The two H atoms evidenced as black balls formerly belonged to the same $H_2O$ molecule.

configuration around $Mg^{2+}$ (upper panel of Figure 6) or the chemistry of the $P-O^{5'}$ bond cleavage in our ribozyme system.

By inspecting the electronic structure, we first remark that an empty state, whose dominant contribution is the $Mg^{2+}$ 3s orbital, appears in the original HOMO−LUMO gap of the anion without $Mg^{2+}$. This gap state is now the LUMO of the present system. The HOMO−LUMO gap changes considerably along the reaction coordinate. While a value of $0.20 \pm 0.03$ and $0.11 \pm 0.02$ eV characterized the reactant and the TS, respectively, it enlarges to $1.63 \pm 0.35$ eV on the product side when the cleavage is completed. The p$\pi$ orbital of $O^{5'}$ hybridizes with the $Mg^{2+}$ 3s orbital to form the LUMO (Figure 6, upper panel) implying a reduction in the p electron density on $O^{5'}$ (Table 2) and thus weakening the $P-O^{5'}$ bond.

It can then be inferred that the divalent metal cation acts as a Lewis acid and its presence is essential in tuning the reaction, in lowering the activation barrier, and in catalyzing the desired bond cleavage, as experiments both in vitro and in vivo seem to suggest.[29,30]

**3. The Role of the Solvent.** We immersed the anionic ribozyme system in a 62-water molecule system as mentioned in the Computational Method section. In the hydrated ribozyme (but in the absence of a metal catalyst), small conformational changes were observed during the equilibration phase: the IMHB between the $O^{2'}H$ and $O^a$ was rapidly broken and these O and H atoms formed H-bonds with nearby water molecules as in Figure 7a. In addition, very stable H-bonds were also formed by $O^a$ and $O^b$ that turned out to be strongly hydrophilic. In fact, each of them formed two H-bonds with water molecules that were found to be rather long living. These H-bonds are characterized by an average lifetime $\tau_{HB} = 1.6 \pm 0.4$ ps.[34] Sometimes, during the dynamics, a third H-bond appears on either $O^a$ and $O^b$ with a shorter lifetime ($0.6 \pm 0.2$ ps). While the lifetime of a normal linear H-bond in liquid water is ~1.0 ps,[35] in our case, $\tau_{HB}$ was ~60% larger, indicating that the ribozyme could form a stronger H bonding to the solvent.

After the equilibration of the system, we performed a constrained dynamics similar to that performed in a vacuum, assuming, consistently, the same reaction coordinate. We computed the activation barrier and found that rather large values were required for the formation of the TBP ($\Delta E = 59.6 \pm 2.5$ kcal/mol and $\Delta F = 57.5 \pm 2.2$ kcal/mol). Then a metastable structure appeared (Figure 7b) located below the absolute maximums by 4.1 and 1.6 kcal/mol for $\Delta E$ and $\Delta F$, respectively. The reaction, from this point, proceeds toward the transesterification (Figure 7c) by overcoming a barrier $\Delta E = 2.4$ kcal/mol and $\Delta F = 1.6$ kcal/mol, which agrees with estimates reported in refs 10 and 11. As expected, a proton is spontaneously transferred from a $H_2O$ molecule to $O^{5'}$ with the subsequent formation of an $OH^-$ radical and a $HO-CH_3$ unit.

The following two results are worthy of note. First, in the solvated anionic system, the pseudorotation was prevented, on the time scale of the simulation, even in the absence of catalytic metal ions. The reason is that $O^a$, $O^b$, and $O^{5'}$ atoms, form H-bonds with the solvent. Therefore, these bonds have to be either broken or switched away. Thus, this reaction path differs from the analogous one (without the metal catalyst) observed in a vacuum. More realistically, it can be argued that the pseudorotation is not totally hindered but requires a time much longer than the one affordable by the simulation to occur. Strong H-bonds were also formed by reaction of $O^a$ and $O^b$ with $H_2O$ molecules, and this retarded the proton transfer—with respect to the reaction in a vacuum—from $O^{2'}$ to $O^a$ until the TBP was formed (reaction coordinate value, 1.87 Å). This might help to address the question about whether the phosphodiester is activated by a proton transfer prior to or simultaneously with the nucleophilic attack.[1,2] It depends on the degree of hydration and, as discussed later, on the presence or absence of a divalent metal ion. In water at ambient conditions and in the absence of a metal catalyst in the vicinity of $O^{2'}$, the proton transfer and the nucleophilic attack seem to occur simultaneously. Second, since H-bonds with water molecules have to be broken in order to allow $O^{2'}$ to start the nucleophilic attack and to form a new bond with P, a very large activation barrier (~60 kcal/mol) makes this process very difficult in the absence of a metal catalyst. Thus, the role of the divalent metal ion, also in solution, is to reduce this energy barrier. This is consistent with the experimental evidence.[31]

Furthermore, the simulation suggests that, contrary to the mechanism proposed by Lim and Tole,[29] which holds in a vacuum, in water the proton transfer from $O^{2'}$ to $O^a$ does not occur directly, but via a *proton wire* mechanism[15] that involves nearby water molecules—two in the present case—that form a H-bond chain between $O^{2'}$ to $O^a$ (Figure 8a). The number of $H_2O$ monomers involved in the process may be different for

(34) The geometrical definition of H-bond adopted is $H-O_{acceptor} < 2.45$ Å and $O_{donor}HO_{acceptor} > 90°$. See, for example: Boero, M.; et al. *Phys. Rev. Lett.* **2000**, *85*, 3245.
(35) Bergman, D. L. *Chem. Phys.* **2000**, *253*, 267.

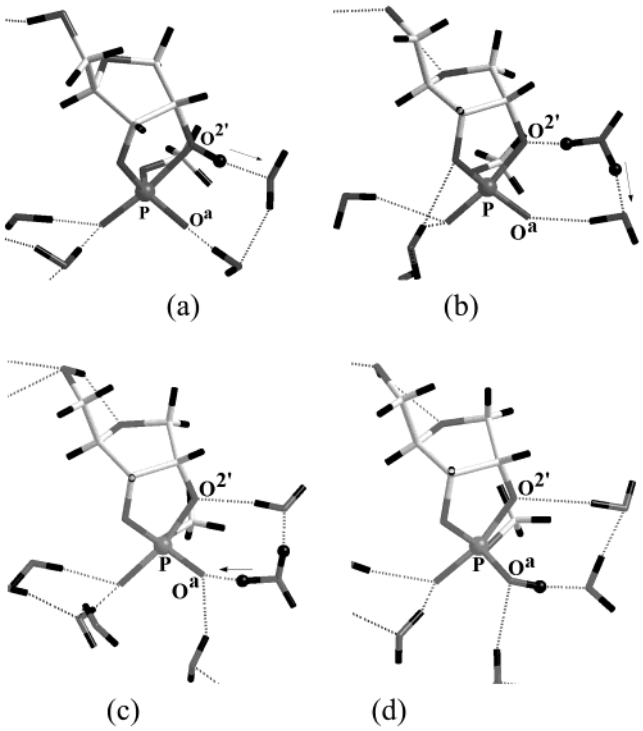


***Figure 8.*** Proton transfer from $O^{2'}$ to $O^a$ mediated by water: the initial configuration (a), the first $H^+$ jump from $O^{2'}$ to the neighbor water molecule (b), the following jump to the next $H_2O$ molecule (c), and the final state (d). The small arrows indicate the direction along which the proton is transferred. The jumping proton is evidenced as a black ball, and only the relevant atoms are labeled.

native larger ribozymes, but the basic mechanism is likely to be the same. The proton initially jumps from $O^{2'}$ to a neighbor H-bonded water molecule that becomes $OH_3^+$ (Figure 8b), then one of the protons of this $OH_3^+$ is transferred to a next H-bonded $H_2O$ molecule in ~0.74 ps (Figure 8c), a number that agrees with previous results on proton diffusion rate in water.[15] This molecule, in turn, becomes a $OH_3^+$ and eventually donates its extra proton to $O^a$ (Figure 8d). The whole $H^+$-transfer process occurs in ~1.91 ps.

**4. The Proton Abstraction from the $O^{2'}H$ Group.** Since the deprotonation of the $O^{2'}H$ group is of fundamental importance in the catalysis of hammerhead ribozyme,[36] we independently investigated the effect of the presence of a divalent metal catalyst ($Mg^{2+}$) in solution. To this aim, we performed a constrained dynamics on our anionic RNA system where the $O^{2'}-H$ distance was assumed as a reaction coordinate; i.e., the $O^{2'}H$ bond was gradually *increased* until the bond breaking occurred. In the absence of $Mg^{2+}$, the computed free energy for the proton abstraction reads $\Delta F_{aq} = 16.5$ kcal/mol, and this initiated a proton wire mechanism analogous to that described in the previous section.

However, this scenario changes drastically in metalloenzymes, i.e., in the presence of $Mg^{2+}$. We put a $Mg^{2+}$ ion close to $O^{2'}$ and performed an unconstrained simulation on this system immersed in the solvent. We noticed that $Mg^{2+}$ reached a dynamically stable position at an average distance of 2.09 ± 0.13 Å from the surrounding $H_2O$ molecules. Note that this configuration could not be stabilized in the absence of the solvent. Here, instead, the metal cation formed a solvation shell

(36) Lyne, P. D.; Karplus, M. *J. Am. Chem. Soc.* **2000**, *122*, 166.

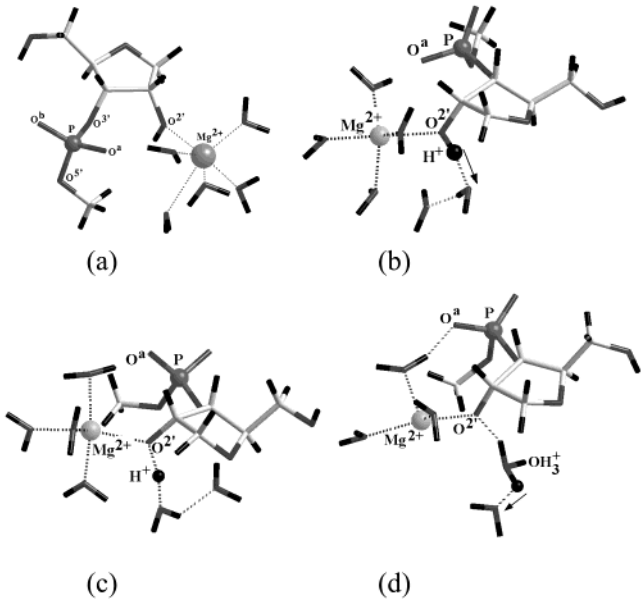


***Figure 9.*** Proton abstraction from $O^{2'}$ in the presence of $Mg^{2+}$: the initial configuration from side (a) and top view (b), the first $H^+$ jump from $O^{2'}$ to the neighbor water molecule (c), and the following jump to the next $H_2O$ molecule (d). The proton, indicated as a labeled black ball, diffuses in the solvent along the directions indicated by the arrows.

of four or five water molecules plus $O^{2'}$ as shown in Figure 9a. As a consequence, the H-bond chain bridging $O^{2'}$ and $O^a$ was interrupted.

Next, we performed a constrained dynamics similar to the previous one and obtained the following results. The presence of the metal enhanced the transfer of the proton of the $O^{2'}H$ group to the next H-bound water molecule (Figure 9b and c), which, in turn, became an $OH_3^+$ (Figure 9d). Then, one of the protons of the $OH_3^+$ was transferred spontaneously to another nearby H-bound molecule and eventually the proton was dispersed in the solvent and diffused away from the ribozyme. Thus, it can be inferred that, in the case of metalloenzymes, the proton transfer is totally hindered, in agreement with the experimental evidence.[16] In this case, the metal catalyst reduces the activation free energy for the deprotonation to $\Delta F_{aq} = 12.6$ kcal/mol.

**5. The Radical System.** Starting from a system similar to the anion (Figure 10a) but in a radical form and sampling the reaction path as in the previous case ($\xi = |P-O^{2'}|$), we observed that the hydrogen transfer (Figure 10b) from $O^{2'}$ to $O^a$ occurs much earlier ($\xi = 3.19$ Å) than in the anionic system. As shown in Figure 11i, the presence of some amount of the hole density on $O^{2'}$ weakens the $O^{2'}-H$ bond, enhancing the transfer process. The proton is initially shared by $O^{2'}$ and $O^a$ in the sense that it jumps from one oxygen to the other several times before stabilizing on $O^a$, keeping an intramolecular H-bond with $O^{2'}$. Then a TBP is formed as shown in Figure 10c. An interesting feature is the fact that the TBP (Figure 10c), corresponding to the first maximum ($\xi = 2.00$ Å) of the free energy (Figure 12), is a TS. This was confirmed also by a normal modes analysis on the average configuration, evidencing one imaginary frequency i149 $cm^{-1}$.

Moving along the reaction coordinate to $\xi = 1.75$ Å, the system goes into a local minimum. This metastable configuration (Figure 10d) has a $P-O^{2'}$ distance slightly shorter than the

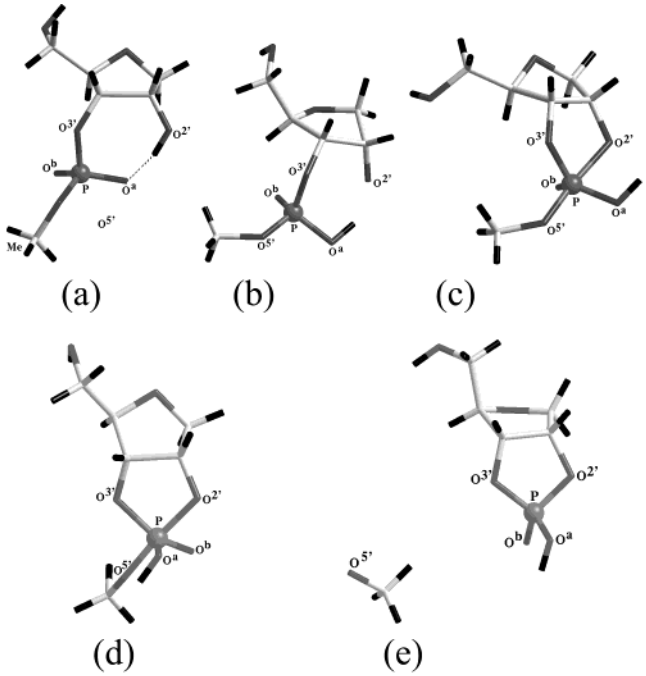


***Figure 10.*** Snapshots of the main phases of the transesterification reaction for the radical system. Before (a) and after (b) the proton transfer from $O^{2'}$ to $O^{a}$, (c) the transition state, (d) the metastable intermediate and (e) the final product.

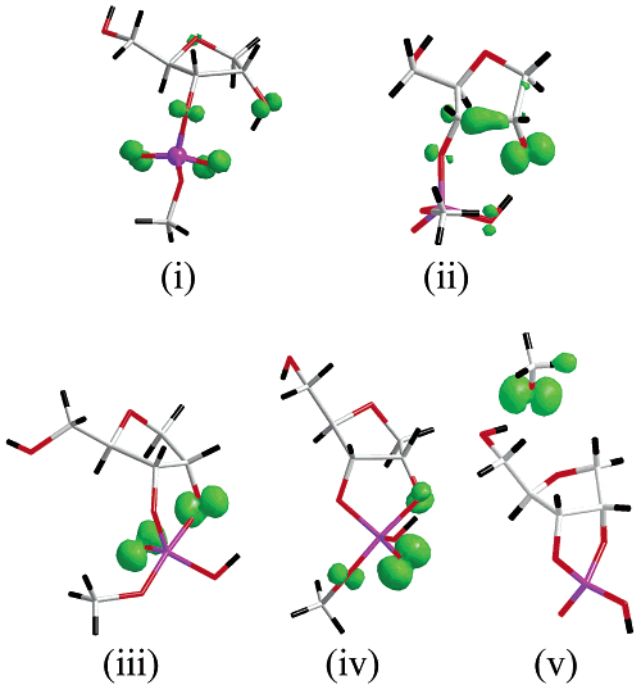


***Figure 11.*** Snapshots of the unoccupied $\beta$ electronic state along the reaction path. The squared modulus wave function is represented as green isosurfaces at a value $6 \times 10^{-4}$ e/Å$^3$. The atomic structure is shown as sticks only with atoms at the crossing points, and the color code for the sticks is the same as in Figure 4.

transition state and its stabilization leads to the breaking of the IMHB between $O^{2'}$ and the H atom bound to $O^{a}$ ($O^{2'}\cdots HO^{a}$). Hence, the position of the H atom is reversed. This local minimum is however very shallow, since a free energy barrier of only 3.2 kcal/mol separates this intermediate from the final product where the $P-O^{5'}$ bond is cleaved. This is in agreement with HF calculations on pentacoordinated oxyphosphorane,[8,9]

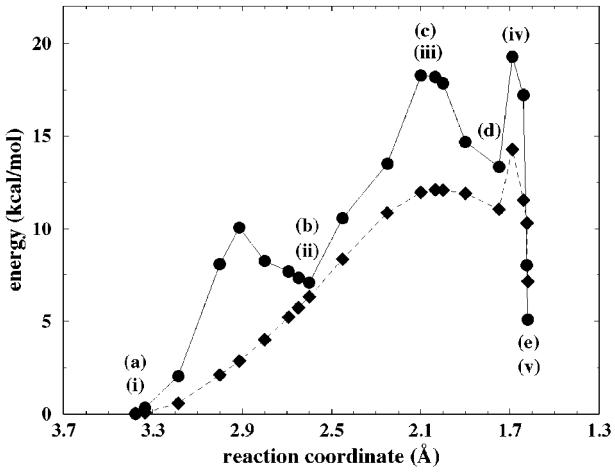


***Figure 12.*** Free (diamonds) and total (circles) energy profiles as a function of the reaction coordinate for the radical system. The labels from (a) to (d) indicate the geometries reported in the snapshots of Figure 7, while labels from (i) to (v) refer to the electronic structure represented in Figure 9 (see text for details).

where a barrier of ~2 kcal/mol is reported. This small barrier is easily overcome by thermal fluctuations and, thereby, the $P-O^{5'}$ bond is cleaved and the $O^{5'}$ group is eventually expelled (Figure 10e).

In the structures from (d) to (e) in Figure 10, $O^{2'}$ and $O^{5'}$ are on average in apical positions. The computed activation energies are $\Delta E = 19.1 \pm 2.4$ kcal/mol and $\Delta F = 14.4 \pm 2.2$ kcal/mol for the total and free energies, respectively. These values are of the same order of magnitude as similar energy barriers reported for methyl hydroxyethyl phosphate (MHEP)[28] and dimethyl phosphate (DMP).[8−10]

To inspect the changes in the electronic structure, we monitored the HOMO and LUMO Kohn−Sham orbitals. Being a radical species, the system is in a doublet spin state having $N + 1$ occupied $\alpha$ states and $N$ occupied $\beta$ states ($N = 41$ in the present case). The separation between the occupied valence band and the empty states band (corresponding to the LUMO of the anionic case) is always rather large (~5.34 eV) along the reaction coordinate, indicating that no mixing of antibonding empty states into the occupied states occurs during the transesterification process.

A feature that deserves attention is the localization of the KS half-occupied state along the reaction path. In particular, the $\beta$ unoccupied state corresponds to a *hole* and displays where the lack of electronic charge is localized. The $\beta$ hole state has a spatial distribution basically similar to that of HOMO in the anionic system shown in Figure 4, as expected; however, some noticeable differences arise because of possible conformational differences. At the beginning, on the reactant side ($\xi = 3.38$ Å), the occupied $\alpha$ orbital is mostly localized on $O^{2'}$ and $O^{3'}$, while its empty $\beta$ counterpart is located on $O^{a}$ and $O^{b}$ with smaller contributions on $O^{2'}$ and $O^{3'}$ (Figure 11i). This indicates a strong tendency of $O^{a}$ and $O^{b}$ to capture electrons in order to fill this empty state. Indeed, this is what partially occurs after the proton transfer from $O^{2'}$ to $O^{a}$ (Figure 11ii). At the TS point, the *hole* is located on the $O^{2'}$ and $O^{b}$ sites (Figure 11iii). The value of the reaction coordinate is still relatively large and the $P-O^{2'}$ bond is not yet fully formed; hence, the localization of the *hole* on $O^{2'}$ accounts for this fact. At the same time, its occupied $\alpha$ counterpart is located mostly on the $O^{5'}$ atom, being

P−$O^{5'}$, a regular chemical bond. No changes in the electronic structure were observed up to the formation of the metastable structure. At this point, the amplitude of the *hole* on $O^{2'}$ gradually decreases while, simultaneously, a contribution arises on $O^{5'}$ (Figure 11iv). This *hole* displacement, i.e., reduction in the number of bonding electrons on $O^{5'}$, leads to the P−$O^{5'}$ bond cleavage (Figure 12v). The Mulliken atomic charges of P and its surrounding oxygen atoms for this transition state, are reported in Table 2.

We acknowledge that the creation of radicals at the cleavage site is difficult in practice and that it could jeopardize the specificity of the ribozyme-mediated transesterification reaction. However, radicals might be created after capture of, for example, Cu ions, leading to redox of the RNA molecules. Hence, a radical system is unlikely in physiologycal conditions; however, *a sufficiently hydrated TBP may exist in any charge state;*[12a,b] *therefore various reaction paths may compete in the actual ribozyme reaction*. The present analyses suggest that *a catalytic metal cation can play a role similar to that of the hole of the radical species*, thus contributing to the selection of the reaction path in vivo.

## Concluding Remarks

We have investigated, via parameter-free dynamical simulation, both the self-cleavage mechanism of RNA enzymes and the competing reaction channel leading to the migration of the phosphodiester after the pseudorotation mechanism. The results of the simulations seem to indicate that the interplay between dynamical motion of the ions and electronic structure modifications occurring during the reaction are crucial in understanding the reaction mechanism. The charge state of the system plays an interesting role in driving the reaction toward the actual transesterification or toward the $3' \rightarrow 2'$ phosphodiester chain transfer. The role of metal cations ($Mg^{2+}$) in enhancing the reaction rate and in preventing pseudorotations in the anionic species has been elucidated, providing support to the mechanism assumed to hold in metalloenzymatic RNA molecules. Furthermore, the effect of a divalent metal ion in the proton abstraction from the $O^{2'}H$ group has been elucidated, elucidating the reasons, supported by experiments, that jeopardize the proton-transfer process. The study presented here, where three different cases are considered, might suggest that the charge state of $O^{5'}$ may be a crucial factor in the selection of the reaction branch.

Our results also allow us to conclude that, due to its multiple roles in the various stages of the transesterification, water is not an inert background, but a very active participant in the reaction mechanism of ribozymes.

**Acknowledgment.** We are grateful to Michele Parrinello, Kazunari Taira, Michiel Sprik, Nicholas C. Handy, Carme Rovira, Yoshitada Morikawa, Hiori Kino, Tadafumi Uchimaru, and Janez Mavri for fruitful discussions and precious suggestions. Calculations were performed on the computers of the Tsukuba Advanced Computing Center (TACC) and of JRCAT. This work was partly supported by New Energy and Industrial Technology Development Organization (NEDO)—Japan.

JA017843Q